# Discovery of *K*-isomeric states in seaborgium isotopes

P. Mošať,[1,*] B. Andel,[2] J. Khuyagbaatar,[1] D. Ackermann,[1,†] S. Antalic,[2] S. Heinz,[1] I. Kojouharov,[1] P. Kuusiniemi,[1,‡] M. Mazzocco,[1,§] J. Mišt,[2] K. Nishio,[3] B. Streicher,[1] B. Sulignano,[1,∥] and F. P. Heßberger[1]
[1]*GSI Helmholtzzentrum für Schwerionenforschung GmbH, 64291 Darmstadt, Germany*
[2]*Department of Nuclear Physics and Biophysics, Comenius University in Bratislava, 84248 Bratislava, Slovakia*
[3]*Advanced Science Research Center, Japan Atomic Energy Agency, Tokai, Ibaraki 319-1195, Japan*

(Received 30 April 2026; accepted 27 July 2026; published 16 September 2026)

The *K*-isomeric states in the heaviest nuclei are among the interesting topics in superheavy-element research. In the present work, we report on the discovery of μs isomers in $^{258,259,260}$Sg which deexcite with half-lives of $120^{+578}_{-55}$ μs, $85 \pm 6$ μs, and $8.5^{+3.1}_{-1.8}$ μs, respectively, and are attributed to high-*K* states formed in multiquasiparticle couplings. In $^{261}$Sg, activity with $12.6^{+2.2}_{-1.6}$ μs half-life was observed and it is suggested to originate from decays of a high-*K* multiquasiparticle and/or single-particle isomeric states.

DOI: 10.1103/gsw6-37t3

## I. INTRODUCTION

Excited nuclear states formed by coupling of quasiparticles may give rise to long-lived isomeric states [1]. This phenomenon occurs when the projection of the total angular momentum onto the symmetry axis, i.e., the *K* quantum number, of a formed state has a large value compared to lower-lying states, including the ground state.

The large difference in *K* reduces the rate of electromagnetic decays [2–4], resulting in longer transition lifetimes relative to the Weisskopf estimates for single-particle transitions [5]. Deexcitation of *K* isomers typically involves the emission of $\gamma$ rays and conversion electrons (CEs) accompanied by x-rays.

These *K*-isomeric states are extensively explored and studied in the regions of medium-mass and heavy-mass nuclei [6,7]. The latter region is of special interest since the deexcitation path of a *K*-isomeric state may differ from that in the medium-mass region, where *K* isomers typically decay via internal electromagnetic transitions. This feature has been experimentally seen in the region of superheavy elements, in the case of $^{270}$Ds ($Z = 110$), observed 25 years ago, where a *K*-isomeric state decays via $\alpha$-particle emission [8]. Moreover, the *K*-isomeric state in this nucleus was found to live longer than the ground state, which renewed interest in the study of this phenomenon in the early 2000s. Since then, extensive experimental programs searching for long-lived *K*-isomeric states decaying via $\alpha$-particle emission have been carried out at various heavy-ion accelerator facilities. So far only one more case has been reported, in $^{266}$Hs ($Z = 108$) [9]. Meanwhile, many *K*-isomeric states with typical electromagnetic deexcitation paths have been discovered in No ($Z = 102$) – Rf ($Z = 104$) isotopes [6,7,10–12]. Among them, three *K* isomers in $^{250}$No [13–16], $^{254}$Rf [17] and $^{252}$Rf [12] with half-lives longer than their spontaneously fissioning ground states were observed. In all cases, direct fission from a *K*-isomeric state was not identified, resulting only in upper limits and showing the strong hindrance of fission caused by the *K* quantum number. In fact, these observations agree with the theoretically anticipated fission stability of the high-*K* states [18,19], which in turn are predicted to exist widely in deformed superheavy nuclei [20–23].

Although this phenomenon is widespread in nobelium and rutherfordium, the occurrence of a *K* isomer in heavier seaborgium (Sg, $Z = 106$) isotopes was only recently reported in $^{259}$Sg [24]. In that work, a CE signal associated with electromagnetic deexcitation of a *K*-isomeric state with a $28^{+126}_{-15}$ μs half-life was measured using fast digital electronics [24]. In recent years, the detection of CEs has been proven to be greatly helpful for the identification of *K*-isomeric states in low-statistics measurements [12,25–28].

In the present work, we explore *K*-isomeric states in Sg isotopes within the existing experimental data from the velocity filter SHIP (Separator of Heavy Ion reaction Products) at GSI, Darmstadt, collected in experiments performed between years 2003 and 2009.

## II. EXPERIMENT

The $^{258–261}$Sg isotopes were produced in the $^{54}$Cr + $^{206–208}$Pb fusion-evaporation reactions. The $\alpha$-decay

*Contact author: p.mosat@gsi.de
†Present address: GANIL, 14076 Caen CEDEX 5, France.
‡Present address: Muon Solutions Oy, Pyhäsalmi, Finland.
§Present address: INFN - Sezione di Padova, 35121 Padova, Italy.
∥Present address: CEA, Centre de Saclay, IRFU/Service de Physique Nucléaire, F-91191 Gif-sur-Yvette, France.

spectroscopy results from these experiments can be found in Refs. [29,30] for $^{261}$Sg, Refs. [31,32] for $^{260}$Sg, and Refs. [32,33] for $^{259}$Sg. The preliminary cross-section values deduced from these experiments are given in [34].

The beam of $^{54}$Cr nuclei was accelerated by the linear accelerator UNILAC to energies of 252–276 MeV and was delivered in a 50-Hz pulsed form (5 ms beam on and 15 ms beam off). Highly enriched $^{206-208}$Pb targets were used.

The evaporation residues (ERs) recoiling from the target were separated in flight from the primary beam, beamlike, and targetlike nuclei by the velocity filter SHIP [35]. The ERs were then directed towards the detection system placed in the focal plane of SHIP [36]. They passed through a time-of-flight (TOF) detector system [37], which served to distinguish implantation signals from decays. In combination with the implantation detector (discussed below), the TOF detectors also allowed discrimination of ERs from scattered projectiles, recoiling target nuclei, and products from transfer reactions passing through SHIP (see, e.g., Ref. [38]).

The ERs were implanted into a 300-$\mu$m-thick 16-strip position-sensitive silicon detector (PSSD) with dimensions of $80 \times 35\,\mathrm{mm}^2$, which is referred to as the STOP detector. A typical implantation depth for ERs calculated from the implantation energy in the STOP detector using LISE++ [39] was 6–9 $\mu$m, depending on the reaction kinematics and the use of deceleration foils. Two vertical (top and bottom) positions of each signal detected in the particular strip were independently determined based on the partial amplitudes of signals measured from the top and bottom ends of the strip's resistive layer and the total amplitude. Individual preamplifier signals from the top and bottom ends were processed with two different gains to cover both low-energy (e.g., $\alpha$, CEs) and high-energy (e.g., SF, ER implantation) signals. The low-energy thresholds were optimized and allowed detection of signals down to ≈80 keV.

The resolutions of reconstructed vertical positions (top and bottom) for $\alpha$ particles and implantation signals (and fissions) measured in the low- and high-energy branches were 0.5 and 2 mm, respectively. These values are typically required to be fulfilled for both top and bottom positions when correlations between the events are being established (correlation analysis is explained in Sec. III in detail). However, the condition for spatial correlation often could not be applied to the CEs because their low energies often resulted in the absence of top and/or bottom positions. Therefore, for CE signals we required only the same strip number as the other correlation members (ER, $\alpha$, and SF).

The resolution of the STOP detector was typically 20–30 keV for the $\alpha$ particles from the implanted activity. The detection efficiency for particles escaping the STOP detector was improved by six additional Si detectors of the same type as the STOP detector, assembled in an open-box geometry (referred to as the BOX detector) and mounted in front of the STOP detector (upstream of the beam). The use of the BOX detector increased the geometrical efficiency for full-energy $\alpha$-particle detection from 50–55% (STOP detector only) to 80–85% (STOP + BOX detectors) [38].

A germanium clover detector installed closely behind the STOP detector covered almost $2\pi$ solid angle for detection

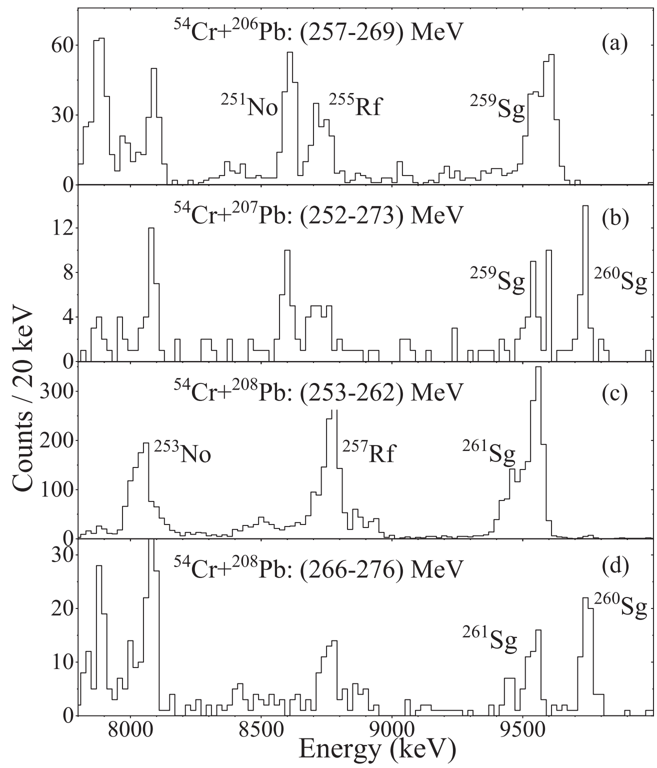


FIG. 1. Low-energy spectra from $^{54}$Cr + $^{206-208}$Pb reactions measured during the beam-off periods in the STOP detector. The reactions and beam energies are given in each panel. Peaks corresponding to the Sg isotopes and their daughter isotopes are marked.

of x-rays and $\gamma$ rays. Depending on the specific experiment, either a VEGA-type detector or the so-called SHIP clover was employed. More details on these detectors, including their absolute efficiency curves, are given in Refs. [31,40].

### III. DATA ANALYSIS

The energy spectra of the STOP detector recorded during the beam-off periods from the three reactions are shown in Fig. 1. Each spectrum consists of data measured at different beam energies which were grouped to highlight the production of a particular Sg isotope. Peaks corresponding to $\alpha$ particles from various Sg isotopes and their daughters are marked.

We established the decay chains for various Sg isotopes by performing position and time correlation searches between the ERs and decays [$\alpha$ and spontaneous fission (SF)] of Sg and their daughters (Rf) and granddaughters (No).

The ER-like events were selected based on their energy in the expected range (20–40 MeV), beam-on period, TOF detector signal, and actual TOF value matching their velocity, as described in Ref. [38]. Possible decays ($\alpha$ or fission) were selected based on their anticipated energy and by being in anticoincidence with the TOF detector.

Candidates for $\alpha$-decay chains were considered according to the known decay properties as events with full energy detected in the STOP or with reconstructed full energy in the STOP + BOX detectors. In addition, escaped $\alpha$ particles, emitted in the backward direction through the BOX detector opening and depositing part of their energy in the STOP detector (typically 0.7–1.2 MeV), were also considered; however, for safe identification of a chain, at least one full-energy $\alpha$ particle (or fission) was required.

The fission candidates were searched for in the energy range of 80–250 MeV. As the fission fragments have opposite directions, the detection efficiency for identifying a fission event by detecting at least one fragment in the STOP detector (although without the full total kinetic energy) was considered to be 100% (see, e.g., [25]).

Once the ER-$\alpha$/SF chains were established, we searched for low-energy signals (CE-like) occurring after each ER signal within 1 ms.

The capability of the detection setup to measure and correlate low-energy signals, such as CEs from the deexcitation of *K*-isomeric states with µs–ms half-lives in the beam-on period, was tested and confirmed by the observation of CEs with energies of ≈120 and ≈140 keV from the decays of the known 50- and 23-µs single-particle isomeric states in $^{255}$Rf [33] and $^{253}$No [30,41,42], respectively, which were populated in the $\alpha$ decays of $^{259}$Sg and $^{261}$Sg.

Prior to the search for *K* isomers in Sg via ER(Sg)-CE-$\alpha$/SF correlations, we first estimated the random time distribution of CE-like events with energies <1.2 MeV. ER-like events also contain implantation signals of target-like transfer-reaction products that may be populated in an isomeric state, which may introduce correlated CEs of nonrandom and non-ER origin. Therefore, we used other beam-related implantation events, for which no real correlated CEs were expected [38]. Their rate was comparable to that of ER-like events. The results for the experiment in which the STOP detector counting rate was the highest are shown in Fig. 2(a). Within the CE search time of 10 ms, the time distribution of the random events is not fully reconstructed, as the mean random correlation time was expected to be longer. This search resulted in $5 \times 10^{-4}$ randomly correlated CE-like events per one ER-like event within 1 ms.

As the rates of ER-like events and CE-like events varied slightly from one experiment to another, we evaluated the random rate for each experiment individually. The random correlation probability was in the range of $(1–5)\times10^{-4}$. These results confirm the capability of the setup to detect CEs originating from possible *K*-isomeric states in the µs–ms range.

When the correlation times of the CEs are short and close to the data acquisition (DAQ) dead time, the time distributions constructed from the directly measured individual times $\Delta t_i$ may not properly represent the radioactive decay time distribution [43]. To restore the real radioactive decay time distribution, a dead-time correction of 20 µs was applied to the individual measured times $\Delta t_i$ (i.e., $\Delta t_i - 20$ µs), as was done in [12]. A detailed description of the DAQ dead-time correction method is given in Appendix A.

The time distributions before (black dotted) and after (blue) the correction of the single-particle isomeric states in $^{255}$Rf and $^{253}$No, mentioned above, are shown in Figs. 2(b) and 2(c), respectively. The dead-time-corrected distributions are better described by radioactive decay with half-lives of $45^{+8}_{-6}$ µs and $27 \pm 3$ µs, respectively, which are in good agreement with the

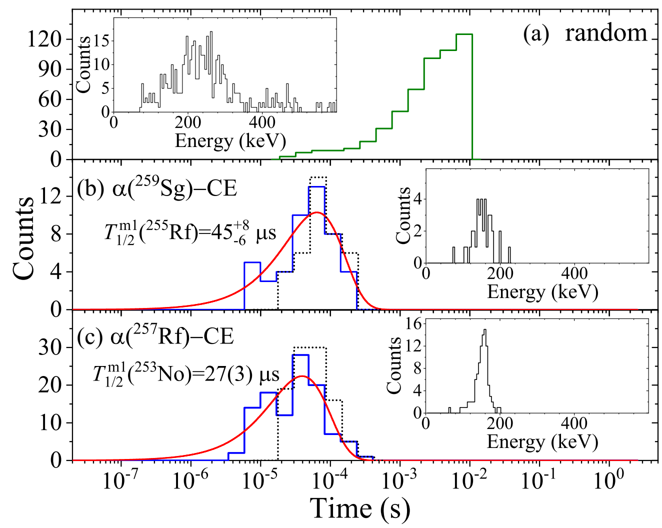


FIG. 2. (a) Time distribution of CE-like events extracted from the time differences between randomly correlated ER-like signals and low-energy signals up to 1.2 MeV. (b) Time distribution of $\alpha(^{259}$Sg)-CE correlations, corresponding to deexcitation of the $5/2^+[622]$ isomeric state in $^{255}$Rf. (c) Time distribution of $\alpha(^{257}$Rf)-CE correlations, corresponding to deexcitation of the $5/2^+[622]$ isomeric state in $^{253}$No. In all panels, the energy distributions of CE-like and CE signals are shown in the inset. In (b) and (c), the black dotted distributions correspond to measured times $\Delta t_i$ and the blue ones correspond to the dead-time-corrected times ($\Delta t_i - 20\ \mu s$). For more details on the dead-time correction, see Appendix A.

literature data [33,41]. In both cases ($^{255}$Rf and $^{253}$No), the CE energies form peaks at ≈120 and ≈140 keV, which correspond to the LMN+ conversion electrons from the decays of single-particle isomeric states with energies of ≈150 and 167 keV, respectively.

We note that the CE energies shown in Figs. 2(b) and 2(c) are corrected for the pole-zero effect, which is caused by the not-yet-restored baseline after a preceding amplified signal from, e.g., $\alpha$ decay or ER implantation. This effect is visible already for the CE energies in $\alpha$-CE correlations and becomes much more significant for ER-CE chains because of the high energies of the ERs. To extract the real energies of CEs, correction factors for the measured energies as a function of correlation time were applied following the procedure of Ref. [25]. In the present work, the correction factors were extracted based on ER-$\alpha$ correlations of the short-lived $^{217}$Th produced in the calibration reactions, and details are given in Appendix B.

## IV. RESULTS AND DISCUSSION

The results of the search for CEs following the ER implantation signals from the identified correlations between ERs and decays of various Sg isotopes, performed as described in Sec. III, are shown in Fig. 3. The measured CE energies are shown as a function of the correlation time for the individual isotopes in different colors. The energies shown in Fig. 3 are not corrected for the pole-zero effect. In the following discussion, CE energies are given after pole-zero correction,

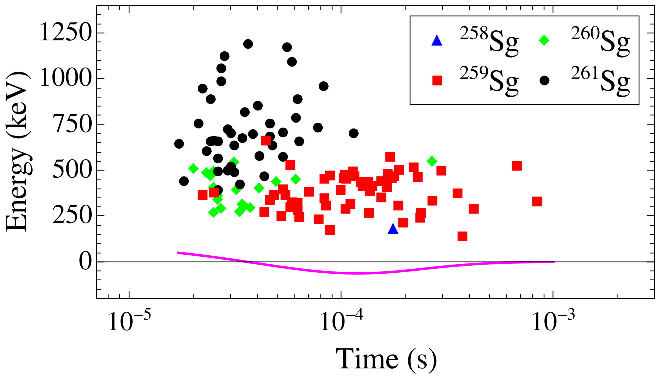


FIG. 3. Energy and correlation time $\Delta t$ of CEs from the ER-CE-$\alpha$ and ER-CE-SF correlations assigned to $^{258}$Sg (blue), $^{259}$Sg (red), $^{260}$Sg (green), and $^{261}$Sg (black). The data points are without the pole-zero correction for energy. The pole-zero effect correction obtained from ER-$\alpha$($^{217}$Th) correlations is shown by the magenta curve (see Appendix B). According to this correction function, the CEs from $^{258}$Sg and $^{259}$Sg with longer half-lives are affected slightly towards the lower energies. On the other hand, most of the events from $^{260}$Sg and $^{261}$Sg are in the $\Delta t_{\text{ER-CE}}$ region where the CE energy becomes affected by the rising ER signal (below 40 µs). The black horizontal line indicates level 0, i.e., no pole-zero correction.

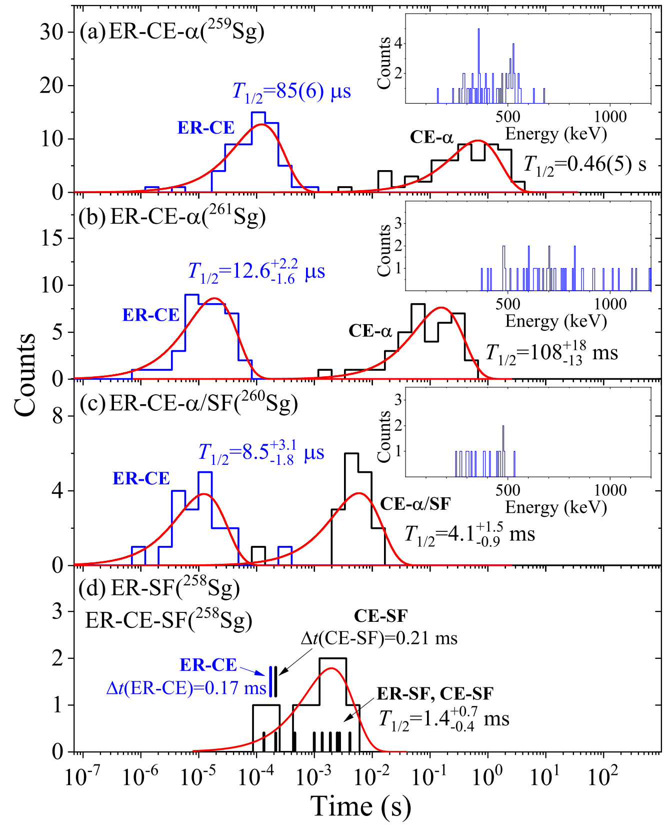


FIG. 4. (a) Distributions of time differences between ER-CE (blue), CE-$\alpha$, and CE-SF (black) from the ER-CE-$\alpha$ and ER-CE-SF correlations assigned to (a) $^{259}$Sg, (b) $^{261}$Sg, and (c) $^{260}$Sg. The energy distributions of CEs are shown in the inset of each of panels (a), (b), and (c). (d) Distribution of time differences of ER-SF correlations and the CE-SF correlation from the ER-CE-SF chain assigned to $^{258}$Sg (black). Individual time differences of each event are shown in black. The time difference of ER-CE from the one ER-CE-SF chain is shown in blue. The time distributions are corrected for the dead time (see Appendix A) and the CE energies are corrected for the pole-zero effect (see Appendix B).

while half-lives are deduced from dead-time-corrected time distributions; the corresponding procedures are described in detail in Appendixes B and A, respectively. A detailed description of the results for the individual Sg isotopes is given in the following subsections.

### A. Isomeric state in $^{259}$Sg

In the present work, the isotope $^{259}$Sg was produced in the $^{54}$Cr + $^{206}$Pb and $^{54}$Cr + $^{207}$Pb reactions via the 1$n$ and 2$n$ evaporation channels, respectively. Corresponding STOP-detector beam-off energy spectra from these reactions are shown in Fig. 1(a) and 1(b). The correlation search between ERs and $\alpha$-particle candidates resulted in a total of 734 ER-$\alpha$ events (with full-energy $\alpha$ particles), which were attributed to the $\alpha$ decay of $^{259}$Sg.

In 54 cases, the ERs were followed by a CE-like signal, i.e., forming ER-CE-$\alpha$($^{259}$Sg) chains. The time distributions of CE and $\alpha$($^{259}$Sg) events relative to the preceding events are shown in Fig. 4(a). Additionally, we found five cases of ER-CE-$\alpha$(escape) chains, in which a low-energy signal following the CE was attributed to an escaped $\alpha$ particle from $^{259}$Sg and was followed by a full-energy $\alpha$ or fission of the daughter ($^{255}$Rf) and/or a full-energy $\alpha$ from the granddaughter ($^{251}$No). These chains are also included in Fig. 4(a).

The half-life of the $\alpha$-decay events was deduced as 0.46(5) s, which is in agreement with the reported value for the $11/2^-$ ground state from Ref. [33]. The time distribution of the CEs shows a well-separated group of events with much shorter $\Delta t$ than the random correlations [cf. Figs. 4(a) and 2(a)]. Moreover, according to the estimated rate of random CE-like signals, only 0.17 randomly correlated CE-like events were expected within a time window of 1 ms after the ER. Therefore, all of these CEs were attributed to an activity with a half-life of 85(6) µs.

The energy distribution of the CEs is plotted in the inset of Fig. 4(a). The corrected CE energies extend up to 0.7 MeV. No prompt $\gamma$ or x-rays were observed in coincidence with the CEs. Based on the CE-energy distribution, an excitation energy of at least 0.7 MeV can be estimated for the isomeric state. Such broad energy distributions are typical for the CEs from the decay of $K$-isomeric states in No–Rf isotopes (see, e.g., the $K$-isomeric states in $^{255}$Rf identified at SHIP under the same experimental conditions [25]), in contrast to the CEs from single-particle isomers [see Figs. 2(b) and 2(c)]. This already suggests that the observed 85(6)-µs activity is associated with a $K$-isomeric state in $^{259}$Sg.

Theory predicts three-quasiparticle states with various configurations at energies above 1 MeV [22,23]. Within the present data, we are unable to determine the $K$ number of the isomeric state. However, the decay scheme allows us to determine which of the two $\alpha$-decaying states in $^{259}$Sg was

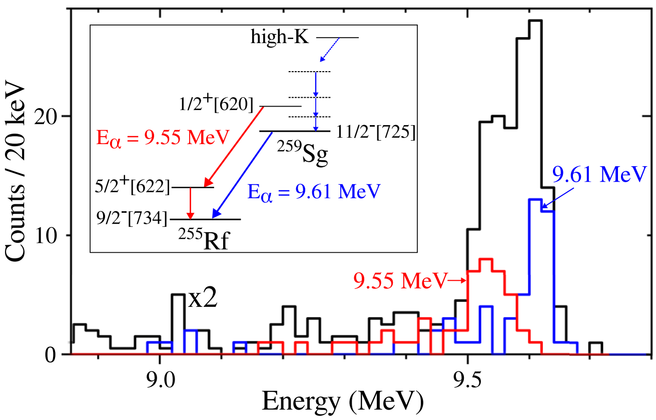


FIG. 5. Energy spectra of $\alpha$ particles from the decay of $^{259}$Sg. Black: all $\alpha$ particles assigned to $^{259}$Sg, downscaled by a factor of 2. Blue: $\alpha$ particles of $^{259}$Sg correlated with ER implantation and preceded by a CE signal, i.e., ER-CE-$\alpha$($^{259}$Sg) correlations. Red: $\alpha$ particles of $^{259}$Sg correlated with ER implantation and followed by a low-energy CE signal, i.e., ER-$\alpha$($^{259}$Sg)-CE correlations. Also shown is the decay scheme of $^{259}$Sg based on Ref. [33], extended by the *K*-isomeric state observed in this work and its proposed deexcitation path.

populated by the deexcitation of the *K*-isomeric state, namely the $11/2^-[725]$ ground state or the $1/2^+[620]$ single-particle isomeric state.

The $\alpha$ decay of the $1/2^+[620]$ single-particle isomer in $^{259}$Sg populates the low-lying $5/2^+[622]$ single-particle isomer in $^{255}$Rf, which in turn deexcites via emission of low-energy CEs (see Sec. III and the decay scheme in Fig. 5). Indeed, when ER-$\alpha$($^{259}$Sg)-CE correlations are selected, the $\alpha$-decay energy of 9.55 MeV (shown in red in Fig. 5) is consistent with the $1/2^+[620] \xrightarrow{\alpha} 5/2^+[622]$ transition between $^{259}$Sg and $^{255}$Rf [33]. On the other hand, the $\alpha$ particles preceded by the higher-energy CEs with the 85-μs half-life (shown in blue in Fig. 5), have higher energies of 9.61 MeV, in agreement with the decay scheme where they are attributed to the $11/2^-[725] \xrightarrow{\alpha} 9/2^-[734]$ transition between $^{259}$Sg and $^{255}$Rf [33] (see inset in Fig. 5). We did not observe any ER-CE-$\alpha$($^{259}$Sg)-CE correlations.

Thus, the deexcitation of the newly observed high-lying isomeric state proceeds to the high-spin $11/2^-$ ground state. Its origin is therefore likely a high-*K* configuration formed by the coupling of three quasiparticles. Taking into account both the CE-energy distribution and the observed $\alpha$-decay pattern, we attribute the 85(6)-μs activity to a *K*-isomeric state in $^{259}$Sg. This result confirms the existence of the *K* isomer reported in Ref. [24], for which a half-life of $28^{+126}_{-15}$ μs was extracted. Such an observation is consistent with the known three-quasiparticle states in the lighter isotones $^{257}$Rf [44–47] and $^{255}$No [11,26]. We note that unambiguous assignments of the nuclear configurations of these isomers have not yet been given.

### B. Isomeric state in $^{261}$Sg

The isotope $^{261}$Sg was produced in the $^{54}$Cr + $^{208}$Pb reaction via the $1n$ evaporation channel. In Figs. 1(c) and 1(d), the beam-off energy spectra of the STOP detector containing the $\alpha$-decay events of $^{261}$Sg are shown. In total, we found 3003 ERs correlated with full-energy $\alpha$ particles (including STOP + BOX events) which were attributed to $^{261}$Sg.

In 30 cases, a CE-like signal was found to follow the ER signal, i.e., ER-CE-$\alpha$($^{261}$Sg) correlations. In addition, we found 14 cases of ER-CE followed by escaped $\alpha$($^{261}$Sg) and full-energy $\alpha$($^{257}$Rf) or $\alpha$($^{253}$No). The time distributions of $\alpha$($^{261}$Sg) and CE events ($\Delta t - 20$ μs) are shown in Fig. 4(b). The time distribution of the $^{261}$Sg $\alpha$-decay events is well described by a half-life of $108^{+18}_{-13}$ ms. It is worth noting that this value is shorter than the $184 \pm 5$ ms half-life, extracted from all ER-$\alpha$($^{261}$Sg) in the same data [30]. However, within the present data we cannot conclude the presence of a state other than the ground state.

According to the estimated rate of random CE-like signals [see Fig. 2(a)], 0.8 randomly correlated CE-like events were expected within a time window of 1 ms after the ER. The observed CEs therefore have a nonrandom origin and their time distribution corresponds to an activity with a half-life of $12.6^{+2.2}_{-1.6}$ μs, which we attribute to an isomeric state in $^{261}$Sg. No $\gamma$ or x-rays were detected in coincidence with these CEs with energies in the range from 0.4 MeV up to 1.2 MeV. The excitation energy of the 12.6-μs isomeric state can be roughly estimated as $E^* > 1.2$ MeV. Such high excitation energy suggests that the isomer may originate from a state with high-*K* multiquasiparticle configuration, which is also supported by the theoretical predictions [22,23].

An isomer with a half-life of $9.0^{+2.0}_{-1.5}$ μs was previously observed in $^{261}$Sg [45], and the $12.6^{+2.2}_{-1.6}$ μs half-life from present results is in agreement with this value. The CE energies measured in [45] were grouped around 200 keV and the isomer was assigned to the single-particle $11/2^-[734]$ state. Surprisingly, the corrected-energy distribution of the presently measured CEs does not show such a peak [see Fig. 4(b)].

At first glance, this discrepancy could be due to an underestimation of the pole-zero correction at very short correlation times (see Appendix B), which could worsen the CE-energy resolution and smear out a narrow peak. However, considering the well-established response of the SHIP detection system and the evaluated correction function for the pole-zero effect (magenta curve in Fig. 3), we do not expect CE energies originating from a 200 keV internal transition to be shifted and broadened to the extent observed in Fig. 3. Therefore, the presently measured CEs spectrum indicates rather a *K*-isomer origin, while we do not exclude the partial presence of the single-particle isomer reported in Ref. [45].

If a second isomeric state in $^{261}$Sg has a high-*K* multiquasiparticle origin, as discussed above, then it should deexcite into a high-spin single-particle state analogous to the case of $^{259}$Sg discussed in the previous subsection. Since the high-spin $11/2^-$ state was assigned to the single-particle isomeric state, deexcitation of higher-lying *K* isomer via the single-particle isomeric state would be probable. We therefore searched for ER-CE-CE-$\alpha$($^{261}$Sg) correlations. No such event was observed, which may, however, be due to the low statistics and DAQ dead time. Therefore, we could not confirm the presence of both isomers in our data.

Finally, we suggest that two isomeric states may exist in $^{261}$Sg, based on the measured CE energies and the present results on $^{259}$Sg, where a $K$-isomeric state was unambiguously identified in addition to the known single-particle isomer.

### C. Isomeric state in $^{260}$Sg

The $^{260}$Sg isotope was produced in the $^{54}$Cr + $^{208}$Pb and $^{54}$Cr + $^{207}$Pb reactions via the $2n$ and $1n$ evaporation channels, respectively. Based on its characteristic $\alpha$-decay energy, $^{260}$Sg can be well separated from $^{259}$Sg and $^{261}$Sg in the $\alpha$ spectra shown in Figs. 1(b) and 1(d).

Compared to the $^{259}$Sg and $^{261}$Sg isotopes, the even-even $^{260}$Sg nucleus has a notable spontaneous-fission branch, and therefore we also searched for ER-SF sequences.

In this case, one has to account for the dominantly fissioning $\alpha$-decay daughter $^{256}$Rf, which has a similar half-life of 6.7 ms [48]. We therefore inspected all ER-SF events for the presence of a full-energy or escaped $\alpha$ particle between the ER and SF events, i.e., we searched for ER-$\alpha$($^{260}$Sg)-SF sequences in order to distinguish fission of $^{260}$Sg from that of $^{256}$Rf. In total, we identified 469 ER-SF($^{260}$Sg) and 202 ER-$\alpha$($^{260}$Sg) correlations.

In 19 cases, a CE was observed within 1 ms after the ER, resulting in 13 ER-CE-SF($^{260}$Sg), 3 ER-CE-$\alpha$($^{260}$Sg), and 3 ER-CE-$\alpha$(escape)-SF($^{256}$Rf) correlations. The time distribution of the CEs ($\Delta t - 20$ μs) and of the $\alpha$/SF events is shown in Fig. 4(c).

According to the estimated rate of random CE-like signals [see Fig. 2(a)], only 0.1 randomly correlated CE-like events were expected within a time window of 1 ms after the ER. The observed CE activity is therefore of nonrandom origin.

A half-life of $8.5^{+3.1}_{-1.8}$ μs was extracted by fitting the time distribution of the CEs. The measured CE energies are shown in Fig. 3, and the pole-zero-corrected energies are shown in the inset of Fig. 4(c). The corrected energies extend up to 0.5 MeV. No $\gamma$ or x-rays were detected in prompt coincidence with the CEs. Since a single-particle isomeric state is excluded in the even-even nucleus, these delayed CEs are attributed to deexcitation of a $K$-isomeric state in $^{260}$Sg with an excitation energy of at least 0.5 MeV.

Theory predicts several two-quasiparticle high-$K$ states in $^{260}$Sg with both two-proton and two-neutron configurations at excitation energies of ≈1 MeV [18]. The present observation is therefore consistent with the existence of such states. It is worth noting that these $K$-isomeric states were also discussed as possible candidates for $\alpha$ decay [19,49], motivated by the observed $\alpha$ decay from $K$-isomeric states in the heavier nuclei $^{270}$Ds and $^{266}$Hs, as discussed in Sec. I.

In this context, a group of five $\alpha$ decay events with energies around 9.7 MeV and mean lifetime of $0.14^{+0.05}_{-0.03}$ ms was observed. These events were already reported in Ref. [31], where their origin was discussed as a possible $\alpha$ decay of a $K$-isomeric state. However, the half-life of $8.5^{+3.1}_{-1.8}$ μs for the presently observed electromagnetically decaying $K$ isomer does not agree with the above-mentioned value, thus, the CEs are from a different state. Nevertheless, we would still not exclude the existence of two $K$-isomeric states with different half-lives, as is well known in the lighter No-Rf isotopes.

TABLE I. Summary of isomeric states identified in the present work. The numbers of observed CEs ($N$), deduced half-lives ($T_{1/2}$), lower limits of the excitation energy ($E^*$), and suggested origins (m-qp: multiquasiparticle; sp: single-particle) are given.

| Isotope | $N$ | $T_{1/2}$ (μs) | $E^*$ (MeV) | Origin |
|---|---|---|---|---|
| $^{258m}$Sg | 1 | $120^{+578}_{-55}$ | >0.25 | m-qp |
| $^{259m2}$Sg | 58 | $85 \pm 6$ | >0.7 | m-qp |
| $^{260m}$Sg | 19 | $8.5^{+3.1}_{-1.8}$ | >0.5 | m-qp |
| $^{261m}$Sg | 44 | $12.6^{+2.2}_{-1.6}$ | >1.2 | m-qp/sp |

### D. Isomeric state in $^{258}$Sg

The isotope $^{258}$Sg was produced in the $^{54}$Cr + $^{206}$Pb reaction via the $2n$ evaporation channel. Similarly to the case of $^{260}$Sg, we searched for ER-SF correlations and identified 9 ER-SF events with a half-life of $1.4^{+0.7}_{-0.4}$ ms, whose time distribution is shown in Fig. 4(d). One ER was followed by a CE-like signal with an energy of 0.25 MeV after 175 μs. According to the estimated rate of random CE-like signals [see Fig. 2(a)], only 0.004 randomly correlated CE-like events were expected within a time window of 1 ms after the ER. No $\gamma$ or x-rays were detected in prompt coincidence with the CE. Since $^{258}$Sg, like $^{260}$Sg, is an even-even nucleus, we attribute this event to deexcitation of a $K$-isomeric state in $^{258}$Sg.

The time distribution of the nine ER-SF events significantly overlaps with the half-life of $120^{+578}_{-55}$ μs attributed to this new $K$-isomeric state. This behavior is consistent with the rapid decrease in fission half-lives of neutron-deficient nuclei towards lower neutron number, as observed in No [50] and in Rf [12]. In this respect, some fission events with comparably low $\Delta t$ cannot be excluded from originating from direct fission of the same $120^{+578}_{-55}$-μs $K$-isomeric state. However, direct fission from $K$-isomeric states has not yet been unambiguously identified [51]. Therefore, we tentatively attribute all nine SF events to the ground state.

Our value of $1.4^{+0.7}_{-0.4}$ ms for the ground-state half-life is in agreement with the previously reported values of $2.9^{+1.3}_{-0.7}$ ms [48] (10 events), $2.7^{+0.9}_{-0.7}$ ms [52] (9 events), $2.1^{+1.0}_{-0.6}$ ms [53] (9 events), $2.7^{+12.9}_{-1.2}$ ms [24] (1 event), and $2.2^{+2.4}_{-1.0}$ ms [54] (9 events). Since only a handful of $^{258}$Sg nuclei have been produced in different experiments worldwide, we combine all available experimental results and deduce a half-life value of $2.3^{+0.4}_{-0.3}$ ms with improved uncertainty.

## V. SUMMARY AND CONCLUSION

In the present work, we report on the discovery of $K$-isomeric states in $^{259}$Sg, $^{260}$Sg, and $^{258}$Sg with half-lives of $85 \pm 6$ μs, $8.5^{+3.1}_{-1.8}$ μs, and $120^{+578}_{-55}$ μs, respectively. In addition, an isomer with $12.6^{+2.2}_{-1.6}$ μs half-life was observed in $^{261}$Sg. The results are summarized in Table I.

For $^{259}$Sg, the high-$K$ character of the new isomeric state was established from its exclusive deexcitation to the higher-$K$ $11/2^-$ ground state rather than to the lower-$K$ $1/2^+$ single-particle isomeric state.

The new isomeric state in $^{260}$Sg deexcites with a half-life much shorter than the fast $\alpha$ decays discussed in Ref. [31]. Nevertheless, it is not excluded that those $\alpha$ decays originate from another isomeric state with a considerable $\alpha$-decay branch.

In $^{258}$Sg, the new isomeric state was found to decay internally with a half-life only about one order of magnitude shorter than the half-life of its fissioning ground state. Therefore, in view of the time distribution of the ER-SF events, a possible direct-fission branch of the $K$-isomeric state cannot be excluded.

For $^{261}$Sg, the isomeric state was measured to have a half-life very similar to the one reported in Ref. [45] which was attributed to the $11/2^-$ single-particle isomer. However, the CE-energy distribution observed in the present work rather indicates an origin from a high-lying $K$ isomer. At the same time, the partial presence of the previously reported single-particle isomer in the obtained data is not excluded [45].

The present experimental findings confirm the recent report on $K$-isomeric state in $^{259}$Sg [24] and expand the region of known $K$ isomers in superheavy nuclei.

## ACKNOWLEDGMENTS

We gratefully remember and acknowledge our late colleagues S. Hofmann, R. Mann, Š. Šáro, and A. V. Yeremin, who contributed to the experiments. We thank A. N. Andreyev, P. Cagarda, V. F. Comas, Z. Gan, C. Grey-Jones, J. A. Heredia, R.-D. Herzberg, M. Leino, A. G. Popeko, D. Rostron, and J. Uusitalo for their contributions to the nuclear spectroscopy program of SHIP during the period 2003–2009. We further acknowledge the UNILAC staff, as well as the ion-source crew, and the GSI target laboratory. This work was supported by the Slovak Research and Development Agency (Contract No. APVV-22-0282) and the Slovak grant agency VEGA (Contract No. 1/0019/25). The publication was funded by the Open Access Publishing Fund of GSI Helmholtzzentrum für Schwerionenforschung.

## DATA AVAILABILITY

The data that support the findings of this article are not publicly available. The data are available from the authors upon reasonable request.

## APPENDIX A: THE RADIOACTIVE DECAY TIME DISTRIBUTION: THE DEAD-TIME CORRECTION

In the SHIP experiment, any subsequent signal above threshold arriving within the 20-μs DAQ dead time is treated as follows: (a) if it arrives within 5 μs after the ER signal, it is registered together with the first event as a pileup, and its energy is fully or partially summed with that of the first signal; (b) if it arrives later than 5 μs after the ER signal, it is lost. Here, 5 μs corresponds to the hardware-defined coincidence window.

The dead time of 20 μs is comparable to the half-lives of some single-particle and high-$K$ isomeric states in the No–Rf region and therefore reduces the registration efficiency for short correlations such as ER-CE or $\alpha$-CE. In logarithmic time distributions of successfully registered correlations, it also produces a gap below 20 μs. When the half-life is comparable to the dead time, this truncation makes a reliable determination of the half-life difficult, especially in cases of limited statistics.

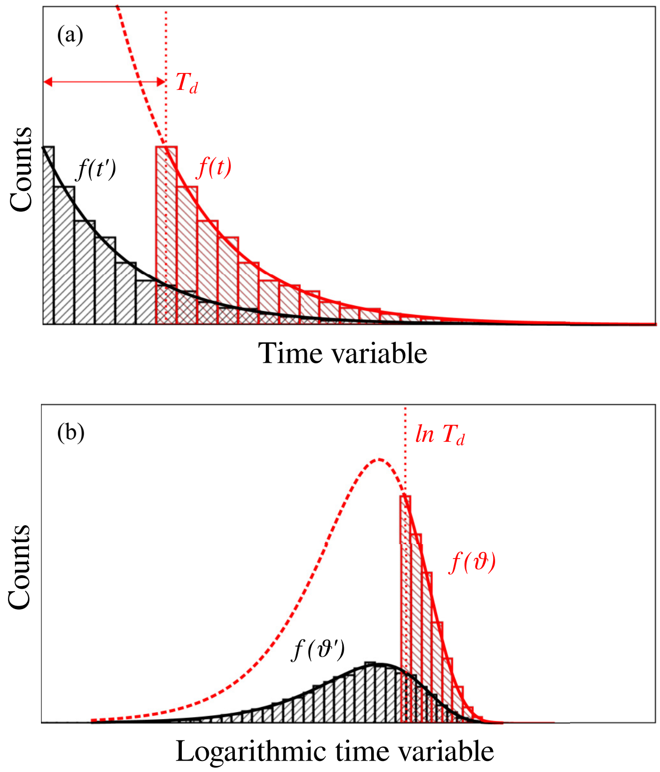


FIG. 6. (a) Randomly generated exponential decay histograms shown as a function of the time variable for the original time $t$ (red) and the shifted time $t' = t - T_d$ (black), together with the corresponding density functions. (b) Same distributions shown as a function of the logarithmic time variable. The red histogram and curve are plotted in the variable $\vartheta = \ln t$, whereas the black histogram and curve are plotted in the corrected variable $\vartheta' = \ln(t - T_d)$.

The decay-time distribution is described by an exponential function,

$$f(t) = Ae^{-\lambda t}, \tag{A1}$$

where $A$ is a normalization constant and $\lambda$ is the decay constant. Such a function is used for fitting decay-time distributions in order to extract the half-life as $T_{1/2} = \ln 2/\lambda$.

In experiments such as those presented in this work, the decay-time distribution is constructed from the measured time differences $t_i$ between two subsequent signals, such as ER, $\alpha$, CE, and SF. Because of the dead time $T_d$, the times $t_i$ are recorded only in the interval $(T_d, \infty)$. To simulate such measurement, we randomly generated a sample of times $t_i$ distributed according to the exponential law with decay constant $\lambda$ and introduced dead time $T_d$. The resulting time distribution is shown in red in Fig. 6(a), and is well described by the function $f(t)$ corresponding to the decay constant $\lambda$. The red dotted part of $f(t)$ corresponds to the inaccessible dead-time region $(0, T_d)$.

Let us now subtract the constant $T_d$ from each $t_i$ of the same data sample. The resulting distribution is shown in black in Fig. 6(a) and is again well described by an exponential function with the same decay constant $\lambda$. This is expected, since one simply replaces the variable $t$ by $t' = t - T_d$, and thus

$$f(t') = f(t - T_d) = Ae^{-\lambda(t-T_d)} = e^{\lambda T_d} f(t). \quad \text{(A2)}$$

This transformation does not affect the estimate of the decay constant $\lambda$ (and thus the half-life $T_{1/2}$): the exponential slope of the distribution remains unchanged, and fitting the original data in $(T_d, \infty)$ by $f(t)$ is equivalent, in terms of the extracted $\lambda$, to fitting the shifted data $t_i' = t_i - T_d$ in $(0, \infty)$ by $f(t')$.

For low-statistics data, time distributions are often displayed in the logarithmic representation proposed in Ref. [43], using the substitution $\vartheta = \ln t$. The corresponding probability-density function is

$$f(\vartheta) = f(e^{\vartheta})\frac{dt}{d\vartheta} = Ae^{\vartheta} e^{-\lambda e^{\vartheta}}. \quad \text{(A3)}$$

This logarithmic representation of the same data sample is illustrated in Fig. 6(b), where the red histogram and curve correspond to the variable $\vartheta = \ln t$. In this representation, the dead time truncates the left tail of the distribution because successfully registered correlation times satisfy $t > T_d$. For the dead-time-corrected times $t' = t - T_d$, the logarithmic variable becomes $\vartheta' = \ln(t - T_d)$. The corrected representation is also shown in Fig. 6(b), where the black histogram and curve correspond to this shifted variable. The corresponding black curve has the same functional form as the original red curve, but is expressed in the corrected variable $\vartheta' = \ln(t - T_d)$. In this way, the same data sample is mapped from the interval $(T_d, \infty)$ to $(0, \infty)$, so that the full shape of the distribution is restored while the decay constant remains unchanged. No additional events are introduced; the data are simply reexpressed in a variable free of the artificial truncation caused by the dead time. The position of the maximum remains unchanged and corresponds to $\ln \tau$, where $\tau = 1/\lambda$.

For the standard exponential distribution, shifting the data by $T_d$ has little practical effect on the fit quality, since the shape is unchanged and the same information is retained. In the logarithmic representation, however, the correction restores the full shape of the distribution and increases the number of useful fitting points.

The constant value subtracted from the measured correlation times does not need to be exactly equal to the dead time. Any value $C$ satisfying $t_i - C > 0$ improves the shape of the logarithmic distribution, provided that $C$ is sufficiently close to $T_d$. In practice, $C$ may be chosen slightly smaller than the shortest individual time $t_i$.

## APPENDIX B: THE BASELINE CORRECTION FOR FAST DECAYS

In cases of two subsequent signals separated by very short times (below ≈0.6 ms) and measured in the same channel of the signal-processing electronics, the energy of the second signal is strongly affected by the shape of the preceding signal. In other words, the baseline is not yet restored when the second signal arrives. This effect leads to a systematic under- or overestimation of the measured energy of the second signal, depending on the correlation time. To correct for this effect, the decay of the signal tail toward the baseline, determined by the shaping-amplifier parameters, must be characterized. An empirical correction can be obtained by studying known fast $\alpha$ decays (see, e.g., Ref. [25], where $^{216}$Ac was used).

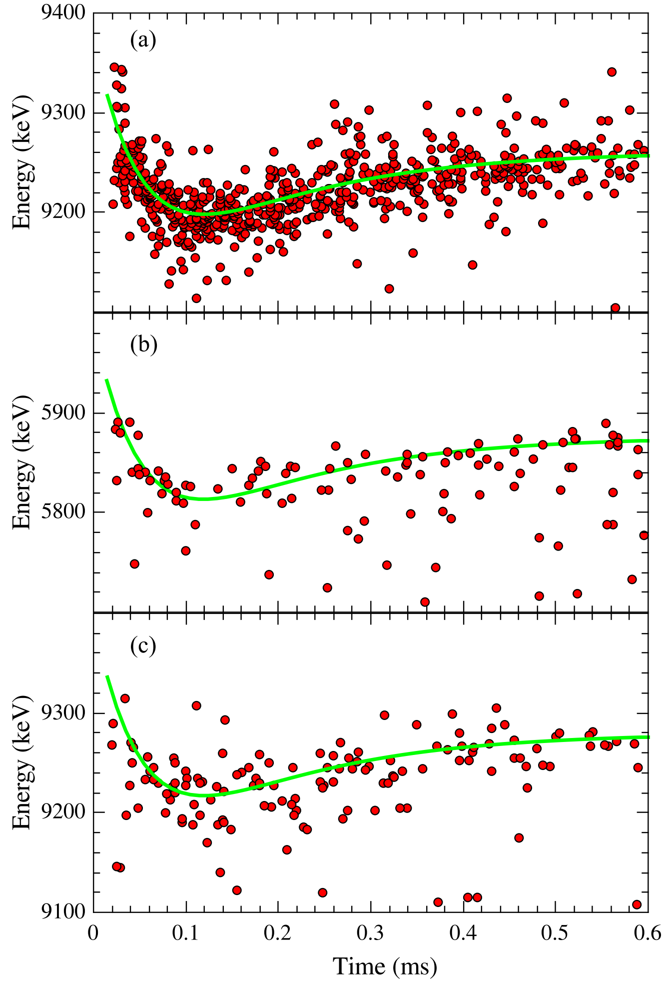


FIG. 7. (a) $E_\alpha$ vs $\Delta t_{\text{ER-}\alpha}$ from the ER-$\alpha$ correlations assigned to $^{217}$Th. Individual red points represent experimentally measured data. Their fit, the green line, represents the time dependence of the measured energies. (b) and (c) represent the same effect as in (a), monitored over the course of the experimental campaign, (b) via ER-$\alpha$($^{211}$At) random correlations and (c) via ER-$\alpha$($^{217}$Th) correlations.

In the experiments presented in this paper, the above-described effect was studied using ER-$\alpha$($^{217}$Th) correlations, where $^{217}$Th ($T_{1/2} = 252$ μs) was produced in the calibration reaction $^{54}$Cr + $^{170}$Er. The measured energies of individual $\alpha$ particles from the correlation pairs are shown as a function of the time difference between the registered ER implantation and the subsequent $\alpha$($^{217}$Th) decay in Fig. 7(a). The experimental data were then fitted to obtain an average correction curve, which was later used for correcting CE energies in ER-CE and $\alpha$-CE correlations from the isomer decays. The correction magnitude is determined by a single scaling parameter proportional to the amplitude of the preceding signal. This parameter multiplies the full correction function and thereby consistently modifies both the peak and the pole-zero undershoot components of the signal response.

During the experimental campaign, the validity of the correction function was further verified using additional ER-$\alpha$($^{217}$Th) correlations, shown in Fig. 7(c), as well as ER-$\alpha$($^{211}$At) and ER-$\alpha$($^{211}$Po) correlations shown in Fig. 7(b). The latter two are of random origin and were observed in cases with an increased rate of transfer products $^{211}$At and $^{211}$Po, which led to an increased probability of random correlations with ER-like events down to the μs range despite their long half-lives. These tests confirmed that the correction function remained valid throughout the experimental campaign.

The correction was applied as an average over all 16 electronic channels, since the available statistics did not allow for channel-by-channel corrections. Although such averaging may lead to some degradation of the resolution, the achieved precision remains on the order of a few tens of keV, as can be seen in Figs. 7(a), 7(b), and 7(c).


[1] P. Walker and G. Dracoulis, Energy traps in atomic nuclei, Nature (London) **399**, 35 (1999).

[2] G. Alaga, K. Alder, A. N. Bohr, and B. R. Mottelson, Intensity rules for beta and gamma transitions to nuclear rotational states, Dan. Mat. Fys. Medd. **29**, 1 (1955).

[3] C. J. J. Gallagher, Classification of beta- and gamma-ray transitions between intrinsic states in deformed even-mass nuclei, Nucl. Phys. **16**, 215 (1960).

[4] A. Bohr and B. R. Mottelson, *Nuclear Structure Volume II: Nuclear Deformations* (W. A. Benjamin, New York, 1975), p. 225.

[5] J. M. Blatt and V. F. Weisskopf, *Theoretical Nuclear Physics* (Springer, New York, 1979).

[6] F. Kondev, G. Dracoulis, and T. Kibédi, Configurations and hindered decays of *K* isomers in deformed nuclei with $A > 100$, At. Data Nucl. Data Tables **103-104**, 50 (2015).

[7] P. M. Walker and F. G. Kondev, *K* isomers in atomic nuclei, Eur. Phys. J. Spec. Top. **233**, 983 (2024).

[8] S. Hofmann, F. P. Heßberger, D. Ackermann, S. Antalic, P. Cagarda, S. Ćwiok, B. Kindler, J. Kojouharova, B. Lommel, R. Mann, G. Münzenberg, A. G. Popeko, Š. Šáro, H. J. Schött, and A. V. Yeremin, The new isotope $^{270}$110 and its decay products $^{266}$Hs and $^{262}$Sg, Eur. Phys. J. A **10**, 5 (2001).

[9] D. Ackermann, S. Antalic, M. Block, H. Brand, B. Kindler, J. Khuyagbaatar, B. Lommel, J. Maurer, K. Nishio, S. Nishio, J. Piot, J. Qin, M. Schädel, B. Streicher, B. Sulignano, and A. Yakushev, Discovery of a K-Isomer in $^{266}$Hs, GSI Report No. 2012-1, 2012 (unpublished), p. 208.

[10] D. Ackermann, S. Antalic, and F. P. Heßberger, Isomers in superheavy nuclei, Eur. Phys. J. Spec. Top. **233**, 1017 (2024).

[11] K. Kessaci, B. J. P. Gall, O. Dorvaux, M. Forge, A. Lopez-Martens, R. Chakma, K. Hauschild, M. L. Chelnokov, V. I. Chepigin, A. V. Isaev, A. A. Kuznetsova, O. N. Malyshev, R. Mukhin, J. Piot, A. G. Popeko, Y. A. Popov, E. A. Sokol, A. I. Svirikhin, and A. V. Yeremin, Cascade of high-*K* isomers in $^{255}_{102}No_{153}$, Phys. Rev. C **110**, 054310 (2024).

[12] J. Khuyagbaatar, P. Mosat, J. Ballof, R. A. Cantemir, Ch. E. Düllmann, K. Hermainski, F. P. Heßberger, E. Jäger, B. Kindler, J. Krier, N. Kurz, S. Löchner, B. Lommel, B. Schausten, Y. Wei, P. Wieczorek, and A. Yakushev, Stepping into the sea of instability: The new sub-μ*s* superheavy nucleus $^{252}$Rf, Phys. Rev. Lett. **134**, 022501 (2025).

[13] D. Peterson, B. B. Back, R. V. F. Janssens, T. L. Khoo, C. J. Lister, D. Seweryniak, I. Ahmad, M. P. Carpenter, C. N. Davids, A. A. Hecht, C. L. Jiang, T. Lauritsen, X. Wang, S. Zhu, F. G. Kondev, A. Heinz, J. Qian, R. Winkler, P. Chowdhury, S. K. Tandel, *et al.*, Decay modes of $^{250}$No, Phys. Rev. C **74**, 014316 (2006).

[14] A. Svirikhin, A. Andreev, A. Yeremin, I. Izosimov, A. Isaev, A. Kuznetsov, A. Kuznetsova, O. Malyshev, A. Popeko, Y. Popov, E. Sokol, M. Chelnokov, V. Chepigin, T. Schneidman, B. Gall, O. Dorvaux, P. Brione, K. Hauschild, A. Lopez-Martens, K. Rezynkina, *et al.*, Characteristics of spontaneous fission of $^{250}$No, Phys. Part. Nuclei Lett. **14**, 571 (2017).

[15] J. Kallunkathariyil, B. Sulignano, P. T. Greenlees, J. Khuyagbaatar, C. Theisen, K. Auranen, H. Badran, F. Bisso, P. Brionnet, R. Briselet, A. Drouart, Z. Favier, T. Goigoux, T. Grahn, K. Hauschild, A. Herzan, F. P. Heßberger, U. Jakobsson, R. Julin, S. Juutinen, *et al.*, Stability of the heaviest elements: *K* isomer in $^{250}$No, Phys. Rev. C **101**, 011301(R) (2020).

[16] J. Khuyagbaatar, H. Brand, Ch. E. Düllmann, F. P. Heßberger, E. Jäger, B. Kindler, J. Krier, N. Kurz, B. Lommel, Y. Nechiporenko, Y. N. Novikov, B. Schausten, and A. Yakushev, Search for fission from a long-lived isomer in $^{250}$No and evidence of a second isomer, Phys. Rev. C **106**, 024309 (2022).

[17] H. M. David, J. Chen, D. Seweryniak, F. G. Kondev, J. M. Gates, K. E. Gregorich, I. Ahmad, M. Albers, M. Alcorta, B. B. Back, B. Baartman, P. F. Bertone, L. A. Bernstein, C. M. Campbell, M. P. Carpenter, C. J. Chiara, R. M. Clark, M. Cromaz, D. T. Doherty, G. D. Dracoulis, *et al.*, Decay and fission hindrance of two- and four-quasiparticle *K* isomers in $^{254}$Rf, Phys. Rev. Lett. **115**, 132502 (2015).

[18] F. R. Xu, E. G. Zhao, R. Wyss, and P. M. Walker, Enhanced stability of superheavy nuclei due to high-spin isomerism, Phys. Rev. Lett. **92**, 252501 (2004).

[19] J. Khuyagbaatar, Fission-stability of high-*K* states in superheavy nuclei, Eur. Phys. J. A **58**, 243 (2022).

[20] H. L. Liu, P. M. Walker, and F. R. Xu, Favored configurations for four-quasiparticle *K* isomerism in the heaviest nuclei, Phys. Rev. C **89**, 044304 (2014).

[21] P. Jachimowicz, M. Kowal, and J. Skalski, Candidates for long-lived high-*K* ground states in superheavy nuclei, Phys. Rev. C **92**, 044306 (2015).

[22] G. G. Adamian, N. V. Antonenko, and W. Scheid, High-spin isomers in some of the heaviest nuclei: Spectra, decays, and population, Phys. Rev. C **81**, 024320 (2010).

[23] P. Jachimowicz, M. Kowal, and J. Skalski, Candidates for three-quasiparticle *K* isomers in even-odd Fm–Cn nuclei, Phys. Rev. C **112**, 064317 (2025).

[24] P. Mosat, J. Khuyagbaatar, J. Ballof, R. A. Cantemir, D. Dietzel, C. E. Düllmann, K. Hermainski, F. P. Heßberger, E. Jäger, B. Kindler, J. Krier, N. Kurz, B. Lommel, S. Löchner, M. Maiti, T. K. Sato, B. Schausten, J. Uusitalo, P. Wieczorek, and A. Yakushev, Probing the shell effects on fission: The new superheavy nucleus $^{257}$Sg, Phys. Rev. Lett. **134**, 232501 (2025).

[25] P. Mosat, F. P. Heßberger, S. Antalic, D. Ackermann, B. Andel, M. Block, S. Hofmann, Z. Kalaninova, B. Kindler, M. Laatiaoui, B. Lommel, A. K. Mistry, J. Piot, and M. Vostinar, *K* isomerism in $^{255}$Rf and total kinetic energy measurements for spontaneous fission of $^{255,256,258}$Rf, Phys. Rev. C **101**, 034310 (2020).

[26] A. Bronis, F. P. Heßberger, S. Antalic, B. Andel, D. Ackermann, S. Heinz, S. Hofmann, J. Khuyagbaatar, B. Kindler, I. Kojouharov, P. Kuusiniemi, M. Leino, B. Lommel, R. Mann, K. Nishio, A. G. Popeko, B. Streicher, B. Sulignano, J. Uusitalo, M. Venhart, *et al.*, Decay studies of new isomeric states in $^{255}$No, Phys. Rev. C **106**, 014602 (2022).

[27] J. Khuyagbaatar, A. K. Mistry, D. Ackermann, L.-L. Andersson, M. Block, H. Brand, Ch. E. Düllmann, J. Even, F. Heßberger, J. Hoffmann, A. Hübner, E. Jäger, B. Kindler, J. Krier, N. Kurz, B. Lommel, B. Schausten, J. Steiner, A. Yakushev, and V. Yakusheva, The identification and confirmation of isomeric states in $^{254}$Rf and $^{255}$Rf through conversion electron detection, Nucl. Phys. A **994**, 121662 (2020).

[28] J. Khuyagbaatar, H. Brand, R. A. Cantemir, Ch. E. Düllmann, M. Götz, S. Götz, F. P. Heßberger, E. Jäger, B. Kindler, J. Krier, N. Kurz, B. Lommel, B. Schausten, and A. Yakushev, Isomeric states in $^{256}$Rf, Phys. Rev. C **103**, 064303 (2021).

[29] B. Streicher, Synthesis and spectroscopic properties of transfermium isotopes with Z = 105, 106 and 107, Ph.D. thesis, Comenius University in Bratislava, Slovakia, 2006 (unpublished).

[30] B. Streicher, F. P. Heßberger, S. Antalic, S. Hofmann, D. Ackermann, S. Heinz, B. Kindler, J. Khuyagbaatar, I. Kojouharov, P. Kuusiniemi, M. Leino, B. Lommel, R. Mann, Š. Šáro, B. Sulignano, J. Uusitalo, and M. Venhart, Alpha-gamma decay studies of $^{261}$Sg and $^{257}$Rf, Eur. Phys. J. A **45**, 275 (2010).

[31] B. Sulignano, Search for K isomers in $^{252,254}$No and $^{260}$Sg and investigation of their nuclear structure, Ph.D. thesis, Johannes Gutenberg-Universität Mainz, Germany, 2007 (unpublished).

[32] F. P. Heßberger, S. Hofmann, B. Streicher, B. Sulignano, S. Antalic, D. Ackermann, S. Heinz, B. Kindler, I. Kojouharov, P. Kuusiniemi, M. Leino, B. Lommel, R. Mann, A. G. Popeko, Š. Šáro, J. Uusitalo, and A. V. Yeremin, Decay properties of neutron-deficient isotopes of elements from $Z = 101$ to $Z = 108$, Eur. Phys. J. A **41**, 145 (2009).

[33] S. Antalic, F. P. Heßberger, D. Ackermann, S. Heinz, S. Hofmann, B. Kindler, J. Khuyagbaatar, B. Lommel, and R. Mann, Nuclear isomers in $^{259}$Sg and $^{255}$Rf, Eur. Phys. J. A **51**, 41 (2015).

[34] F. P. Heßberger, S. Antalic, B. Streicher, B. Sulignano, D. Ackermann, M. Block, S. Heinz, S. Hofmann, J. Khuyagbaatar, B. Kindler, I. Kojouharov, B. Lommel, and R. Mann, Cross-sections for production of neutron deficient Sg-isotopes in reactions $^{54}$Cr + $^{206,207,208}$Pb, GSI Report No. 2010-1, 2010 (unpublished), p. 172.

[35] G. Münzenberg, W. Faust, S. Hofmann, P. Armbruster, K. Güttner, and H. Ewald, The velocity filter SHIP, a separator of unslowed heavy ion fusion products, Nucl. Instrum. Methods **161**, 65 (1979).

[36] S. Hofmann and G. Münzenberg, The discovery of the heaviest elements, Rev. Mod. Phys. **72**, 733 (2000).

[37] Š. Šáro, R. Janik, S. Hofmann, H. Folger, F. Heßberger, V. Ninov, H. Schött, A. Kabachenko, A. Popeko, and A. Yeremin, Large size foil-microchannel plate timing detectors, Nucl. Instrum. Methods Phys. Res. Sect. A **381**, 520 (1996).

[38] S. Hofmann, D. Ackermann, S. Antalic, H. G. Burkhard, V. F. Comas, R. Dressler, Z. Gan, S. Heinz, J. A. Heredia, F. P. Heßberger, J. Khuyagbaatar, B. Kindler, I. Kojouharov, P. Kuusiniemi, M. Leino, B. Lommel, R. Mann, G. Münzenberg, K. Nishio, A. G. Popeko, *et al.*, The reaction $^{48}$Ca + $^{238}$U $\rightarrow$ $^{286}$112* studied at the GSI-SHIP, Eur. Phys. J. A **32**, 251 (2007).

[39] O. Tarasov and D. Bazin, LISE++: Radioactive beam production with in-flight separators, Nucl. Instrum. Methods Phys. Res. Sect. B **266**, 4657 (2008).

[40] F. P. Heßberger, S. Antalic, B. Sulignano, D. Ackermann, S. Heinz, S. Hofmann, B. Kindler, J. Khuyagbaatar, I. Kojouharov, P. Kuusiniemi, M. Leino, B. Lommel, R. Mann, K. Nishio, A. G. Popeko, Š. Šáro, B. Streicher, J. Uusitalo, M. Venhart, and A. V. Yeremin, Decay studies of *K* isomers in $^{254}$No, Eur. Phys. J. A **43**, 55 (2010).

[41] A. Lopez-Martens, K. Hauschild, A. V. Yeremin, O. Dorvaux, A. V. Belozerov, C. Briançon, M. L. Chelnokov, V. I. Chepigin, D. Curien, P. Désesquelles, B. Gall, V. A. Gorshkov, M. Guttormsen, F. Hanappe, A. P. Kabachenko, F. Khalfallah, A. Korichi, A. C. Larsen, O. N. Malyshev, A. Minkova, *et al.*, Isomeric states in $^{253}$No, Eur. Phys. J. A **32**, 245 (2007).

[42] S. Antalic, F. P. Heßberger, D. Ackermann, S. Heinz, S. Hofmann, Z. Kalaninová, B. Kindler, J. Khuyagbaatar, I. Kojouharov, P. Kuusiniemi, M. Leino, B. Lommel, R. Mann, K. Nishio, Š. Šáro, B. Streicher, B. Sulignano, and M. Venhart, Isomeric states in $^{253}$No and $^{253}$Fm, Eur. Phys. J. A **47**, 62 (2011).

[43] K. H. Schmidt, C. C. Sahm, K. Pielenz, and H. G. Clerc, Some remarks on the error analysis in the case of poor statistics, Z. Phys. A **316**, 19 (1984).

[44] J. Qian, A. Heinz, T. L. Khoo, R. V. F. Janssens, D. Peterson, D. Seweryniak, I. Ahmad, M. Asai, B. B. Back, M. P. Carpenter, A. B. Garnsworthy, J. P. Greene, A. A. Hecht, C. L. Jiang, F. G. Kondev, T. Lauritsen, C. J. Lister, A. Robinson, G. Savard, R. Scott, *et al.*, Spectroscopy of $^{257}$Rf, Phys. Rev. C **79**, 064319 (2009).

[45] J. S. Berryman, R. M. Clark, K. E. Gregorich, J. M. Allmond, D. L. Bleuel, M. Cromaz, I. Dragojević, J. Dvorak, P. A. Ellison, P. Fallon, M. A. Garcia, S. Gros, I. Y. Lee, A. O. Macchiavelli, H. Nitsche, S. Paschalis, M. Petri, J. Qian, M. A. Stoyer, and M. Wiedeking, Electromagnetic decays of excited states in $^{261}$Sg ($Z = 106$) and $^{257}$Rf ($Z = 104$), Phys. Rev. C **81**, 064325 (2010).

[46] J. Rissanen, R. M. Clark, K. E. Gregorich, J. M. Gates, C. M. Campbell, H. L. Crawford, M. Cromaz, N. E. Esker, P. Fallon, U. Forsberg, O. Gothe, I.-Y. Lee, H. L. Liu, A. O. Machiavelli, P. Mudder, H. Nitsche, G. Pang, A. Rice, D. Rudolph, M. A. Stoyer, *et al.*, Decay of the high-*K* isomeric state to a rotational band in $^{257}$Rf, Phys. Rev. C **88**, 044313 (2013).

[47] P. Mosat, S. Antalic, F. Heßberger, D. Ackermann, B. Andel, M. Block, Z. Kalaninova, B. Kindler, M. Laatiaoui, B. Lommel, A.

Mistry, J. Piot, and M. Vostinar, Isomeric States in $^{255}$Rf, $^{256}$Rf and $^{257}$Rf, Acta Phys. Pol. B **51**, 849 (2020).

[48] F. P. Heßberger, S. Hofmann, V. Ninov, P. Armbruster, H. Folger, G. Münzenberg, H. J. Schött, A. G. Popeko, A. V. Yeremin, A. N. Andreyev, and Š. Šáro, Spontaneous fission and alpha-decay properties of neutron deficient isotopes $^{257-253}$104 and $^{258}$106, Z. Phys. A **359**, 415 (1997).

[49] R. M. Clark and D. Rudolph, $\alpha$ decay of high-$K$ isomers in $^{270}$Ds and $^{266}$Hs in a superfluid tunneling model, Phys. Rev. C **97**, 024333 (2018).

[50] J. Khuyagbaatar, R. Cantemir, C. Düllmann, F. Heßberger, E. Jäger, B. Kindler, J. Krier, N. Kurz, B. Lommel, P. Mosat, B. Schausten, and A. Yakushev, Search for µs-isomers in $^{251-254}$No, Nucl. Phys. A **1070**, 123382 (2026).

[51] A. Lopez-Martens, K. Hauschild, A. I. Svirikhin, Z. Asfari, M. L. Chelnokov, V. I. Chepigin, O. Dorvaux, M. Forge, B. Gall, A. V. Isaev, I. N. Izosimov, K. Kessaci, A. A. Kuznetsova, O. N. Malyshev, R. S. Mukhin, A. G. Popeko, Y. A. Popov, B. Sailaubekov, E. A. Sokol, M. S. Tezekbayeva, *et al.*, Fission hindrances in transfermium nuclei, EPJ Web of Conf. **290**, 02027 (2023).

[52] J. B. Patin, Experimental cross sections for reactions of heavy ions and $^{208}$Pb, $^{209}$Bi, $^{238}$U, and $^{248}$Cm targets, Ph.D. thesis, University of California, Berkeley, 2002.

[53] C. M. Folden III, I. Dragojević, Ch. E. Düllmann, R. Eichler, M. A. Garcia, J. M. Gates, S. L. Nelson, R. Sudowe, K. E. Gregorich, D. C. Hoffman, and H. Nitsche, Measurement of the $^{208}$Pb($^{52}$Cr, $n$)$^{259}$Sg excitation function, Phys. Rev. C **79**, 027602 (2009).

[54] A. V. Isaev, R. S. Mukhin, A. V. Andreev, A. Rahmatinejad, T. M. Shneidman, V. I. Chepigin, V. D. Danilkin, H. M. Devaraja, A. Ismailova, I. N. Izosimov, A. A. Kuznetsova, O. N. Malyshev, Y. A. Popov, B. Sailaubekov, E. A. Sokol, M. S. Tezekbayeva, I. I. Ulanova, and A. I. Svirikhin, Prompt neutron emission in the spontaneous fission of $^{258,260}$Sg, JINR Preprint E7-2026-3, 2026 (unpublished).